

https://doi.org/10.1070/QEL17208

Structural and optical properties of nanoparticles formed by laser ablation of porous silicon in liquids: Perspectives in biophotonics

S.V. Zabotnov, D.A. Kurakina, F.V. Kashaev, A.V. Skobelkina, A.V. Kolchin, T.P. Kaminskaya, A.V. Khilov, P.D. Agrba, E.A. Sergeeva, P.K. Kashkarov, M.Yu. Kirillin, L.A. Golovan

Abstract. **The paper discusses the possibility of manufacturing silicon nanoparticles, which are suitable for contrasting biological tissues imaged by optical coherence tomography, by femtosecond laser ablation of porous silicon in various liquids. The manufactured nanoparticles are characterised by average sizes of 87, 112, and 102 nm for cases of ablation in water, ethanol, and liquid nitrogen, respectively, as well as a relatively narrow size distribution, which provides additional advantages for subsequent delivery into biological tissues. Electrochemical etching, which results in the formation of layers of porous silicon, allows the yield of ablation products to be increased several-fold by lowering the ablation threshold, thereby increasing the light scattering efficiency of the prepared suspensions compared with the case of using crystalline silicon as targets. The possibility of obtaining high-contrast images of a biotissue phantom based on an agar gel with embedded nanoparticles is shown. The magnitude of the contrast depends on the liquid used for ablation and correlates with the values of the reduced scattering coefficient of the studied suspensions.**

Keywords: *silicon nanoparticles, laser ablation in liquids, atomic force microscopy, light scattering, spectrophotometry, optical coherence tomography.*

1. Introduction

Silicon nanoparticles (SNPs) are promising agents for optical imaging and laser therapy due to their low toxicity and high speed of particle release from the organism [1–5]. However, for the effective use of SNPs as such agents, it is necessary to be able to control the physical properties of particle suspensions at the stage of their manufacturing. Thus, the use of SNPs as contrasting agents for optical diagnostic techniques based on light scattering requires a high scattering coefficient of the employed nanoparticle suspensions, as well as a high scattering cross section of individual particles [6, 7]. For the use of SNPs as contrasting agents in imaging modalities, where the contrast is based on the difference in absorption coefficients [8], as well as for therapeutic applications, such as photohyperthermia [9–11] and photodynamic therapy [12–14], the absorption coefficient of the SNP suspension is important. The use of SNPs in fluorescence diagnostic techniques [1, 15] requires high photoluminescence efficiency.

The general requirement consists in a sufficiently small size of the nanoparticles (no more than 100 nm), which is a condition for their effective penetration into tissues upon topical application and free circulation in the bloodflow when administered intravenously. It is important to note that the most common and traditional techniques for manufacturing SNPs are ultrasonic grinding [1, 9, 10, 12–14] and mechanical grinding in planetary mills [5, 11, 15] of porous silicon (PS) layers preformed by electrochemical etching technique [16]. Despite the simplicity and accessibility, the main disadvantage of these techniques is the difficulty of ensuring the small size of the nanoparticles, which is a fundamental limitation of the mechanical grinding technique. Usually particles with an average size of more than 100 nm are formed [1, 5, 10, 13].

An alternative technique allowing smaller SNPs to be produced is pulsed laser ablation of silicon in liquids [4, 17–20]. The SNPs formed by this technique have a high degree of biocompatibility due to the absence of undesirable chemical impurities [4, 17, 18], and their size can be controlled by the selection of the appropriate buffer liquid for ablation [19, 20]. As a result, the ablation products agglomerate upon collision with liquid molecules (cooling) to SNPs [21], and the nanosystem formed in this way in most cases is a ready-made suspension suitable for further use in different applications.

Pulsed laser ablation technique allows chemically pure SNPs to be formed with a size of less than 100 nm and a relatively narrow size distribution, which, under certain technological conditions of manufacturing, exhibit photoluminescence in the red and near-infrared spectral ranges. This is fundamentally important for using such structures for fluorescence imaging of biological tissues [18, 22, 23] and photodynamic therapy [24]. It should be noted that the efficiency and spectral characteristics of the photoluminescence of SNPs produced by laser ablation are comparable with these parameters for PS-based structures [1, 15, 25, 26] currently used in the above biomedical applications. At the same time, in the case of using SNPs as contrasting agents for visualising a phantom of a biological tissue by optical coherence tomography (OCT), it was previously shown [7] that monocrystalline silicon ablated in water provides a lower image contrast as com-

S.V. Zabotnov, F.V. Kashaev, A.V. Skobelkina, A.V. Kolchin, T.P. Kaminskaya, P.K. Kashkarov, L.A. Golovan Faculty of Physics, Lomonosov Moscow State University, Vorob'evy gory 1, 119991 Moscow, Russia; e-mail: golovan@physics.msu.ru;
D.A. Kurakina, A.V. Khilov, M.Yu. Kirillin Institute of Applied Physics, Russian Academy of Sciences, ul. Ulyanova 46, 603950 Nizhny Novgorod, Russia;
P.D. Agrba Lobachevsky State University of Nizhny Novgorod, prosp. Gagarina 23, 603950 Nizhny Novgorod, Russia; Faculty of Physics, Lomonosov Moscow State University, Vorob'evy gory 1, 119991 Moscow, Russia;
E.A. Sergeeva Institute of Applied Physics, Russian Academy of Sciences, ul. Ulyanova 46, 603950 Nizhny Novgorod, Russia; Faculty of Physics, Lomonosov Moscow State University, Vorob'evy gory 1, 119991 Moscow, Russia

Received 27 November 2019
Kvantovaya Elektronika **50** (1) 69–75 (2020)
Translated by M.Yu. Kirillin

pared to mechanically ground PS with initially high light scattering characteristics.

In this connection, it is important to study the structural and optical properties of SNPs and their suspensions fabricated by laser ablation of PS in liquids aimed at evaluating their potential for contrasting in OCT imaging. It should be noted that the use of PS as a target for ablation is also promising from the point of view of an order-of-magnitude lower ablation threshold for this material as compared to traditionally employed monocrystalline silicon [27], which provides undoubted gain in the amount of ablation products formed under such conditions and, accordingly, the amount of SNPs.

In the frames of this work, we analyse the possibility of controlling the size and efficiency of the formation of SNPs produced by femtosecond laser ablation of porous and crystalline (given for comparison) silicon by selecting the appropriate buffer liquid: water, ethanol, or liquid nitrogen. The light absorption and scattering spectra of SNP suspensions are compared in the wavelength range from 400 to 1000 nm. In an experiment with agar phantoms of biological tissues, the perspectives of using nanoparticle suspensions fabricated by laser ablation of PS for contrasting OCT images are evaluated.

2. Materials and methods

The SNP fabrication was performed in two stages. First, PS layers were prepared by the anodic electrochemical etching technique [16]. Polished p^+ type silicon wafers with a specific resistivity of 17–23 mΩ cm and a crystallographic surface orientation of (100) were used as etching substrates. Prior to etching, these plates were placed for several seconds in 47.5% hydrofluoric acid (HF) to remove natural oxide from the surface. An electrolyte consisting of a solution of hydrofluoric acid and ethanol (C_2H_5OH) in a ratio of 1:1 was used directly for etching. The etching current density was 73 mA cm^{-2}, and the etching time was 30 minutes. With the listed etching parameters, PS layers with characteristic pore sizes of 10–70 nm are formed [7], which allows one to classify the fabricated samples as mesoporous [28]. The thickness of the formed PS films was 110 ± 5 μm according to optical microscopy data.

At the second stage, PS films on the initial monocristalline substrate were used as targets for femtosecond laser ablation performed using an Avesta Cr:forsterite femtosecond laser system based on a master oscillator, regenerative and multipass amplifiers. The main features of the operation of these systems are described in [29, 30]. The parameters of the output pulses of the laser system used in our experiments are following: a wavelength of 1250 nm, a duration of 160 fs, an energy of 0.8–1.0 mJ, and a repetition rate of 10 Hz.

In the case of ablation in distilled water and ethanol, the radiation was focused on a target located in the cell with the corresponding buffer liquid using a lens with a focal length of 40 mm. In order to homogenise the produced SNP suspension during the ablation process, the liquid was mixed using an MM-1 magnetic stirrer. To prevent degeneration of the target during ablation, the cell with the target was shifted perpendicular to the wave vector of the laser beam using two orthogonally oriented automated mechanical translators. In course of SNP formation, the liquid acquired a typical brown colour. Target irradiation times are presented in Table 1. To compare the structural and optical properties of the SNPs formed by laser ablation of PS and crystalline silicon (CS), the latter was also nanostructured by laser ablation under similar conditions. The difference in the experiments consisted in a longer CS irradiation as compared to PS (Table 1), due to above mentioned higher ablation threshold [27] and lower efficiency of SNP production in the first case. It should be noted that longer exposure leads to an increase in the contribution of the so-called laser fragmentation of the formed SNPs in suspension and to a decrease in their size [22]. However, in our experiments, the typical exposure times were quite large and, therefore, even under the assumption of the laser fragmentation process occurrence, its effect on the particle size was comparable in both cases. The main goal of changing the exposure time was to obtain suspensions with comparable mass concentrations of SNPs.

Table 1. Fabrication parameters, average size, standard deviation, and mass concentration of SNPs.

Target material	Buffer liquid	Exposure time/min	Average SNP size/nm	Standard deviation /nm	SNP mass concentration /mg mL^{-1}
PS	Water	120	87	22	0.8
CS	Water	240	80	21	0.5
PS	Ethanol	120	112	26	1.0
CS	Ethanol	240	45	24	0.6
PS	Liquid nitrogen	45	102	16	0.6
CS	Liquid nitrogen	45	16	6	0.4

Ablation in liquid nitrogen was performed when the PS and CS targets were placed in a Petri dish mounted on a wire holder in a thermos with liquid nitrogen. Irradiation was performed after beam focusing with a lens having a focal length of 100 mm. The choice of a lens with a longer focus as compared to the experiments in water and ethanol was due to avoid the effects of liquid nitrogen vapours on the setup optical components. An increase in the focal length of the lens is known to lead to an almost directly proportional increase in the waist radius [31] and, consequently, to a change in the energy density on the irradiated target at a fixed laser pulse energy. In this work, the contribution of this factor to the process of SNP formation in the experiments was not evaluated since it requires for simultaneous account of the extinction of the focused laser beam in various liquids and on ablation products. Moreover, the concentration of these products increased in the course of irradiation.

The irradiation time for experiments in liquid nitrogen in all cases was limited by 45 minutes due to intensive evaporation of this liquid from a thermos. After irradiation, the Petri dish with SNPs was removed from the thermos and filled with distilled water. The resulting suspension was used in further experiments.

The size distribution of the formed SNPs was analysed based on atomic force microscopy (AFM) data obtained with an ND-MDT SolverPRO scanning probe microscope. The sampling size for plotting the corresponding histograms was 200–250 particles for each type of SNPs. The SNP size was evaluated from the height of the peak in AFM profilograms.

The mass concentrations of the fabricated SNPs in suspensions were determined by the gravimetric technique by individually weighing empty plastic cuvettes, cuvettes with suspensions of a known volume, and cuvettes with SNPs after evaporation of liquids. The results are listed in Table 1.

The optical properties of the studied SNP suspensions were determined in the wavelength range of 400–1000 nm based

on measurements of the collimated and diffuse transmission spectra, as well as diffuse reflectance spectra. The measurements were carried out for 5-mm thick SNP suspension layers placed in a quartz cuvette using an Analytik Jena SPECORD 250 spectrophotometer equipped with an integrating sphere. Absorption and scattering coefficients (μ_a and μ_s, respectively), together with anisotropy factor g were reconstructed from the measured spectral dependencies based on the look-up table produced using Monte Carlo simulations [32].

The experiments on imaging of biological tissue phantoms using OCT in the presence of SNPs, which serve as contrast agents, were performed using an OCT-1300E system (centre probing wavelength of 1300 nm, IAP RAS, Biomedtech, Russia). Droplets of SNP suspensions were administered to the surface of a biological tissue phantom represented by a 0.2% agar gel.

3. Results and discussion

Based on AFM data, histograms of the size distribution of the SNPs formed by femtosecond laser ablation of PS and CS in various liquids were calculated (Fig. 1). Regardless of the buffer liquid used, in all cases the values of the average sizes and standard deviation of SNPs produced with PS as a target (Figs 1a, 1c, and 1e) exceed those for CS (Figs 1b, 1d, and 1f) in the case of ablation in the same liquid (Table 1).

The obtained result is easily explained by a decrease in the silicon ablation threshold in the case of PS as compared to CS [27] due to a lower thermal conductivity of the porous matrix in contrast to bulk material and partial destruction of Si–Si bonds in the crystal lattice during electrochemical etching. As a result, in the process of subsequent laser irradiation of the PS layers, the yield of ablation products and, respectively, the

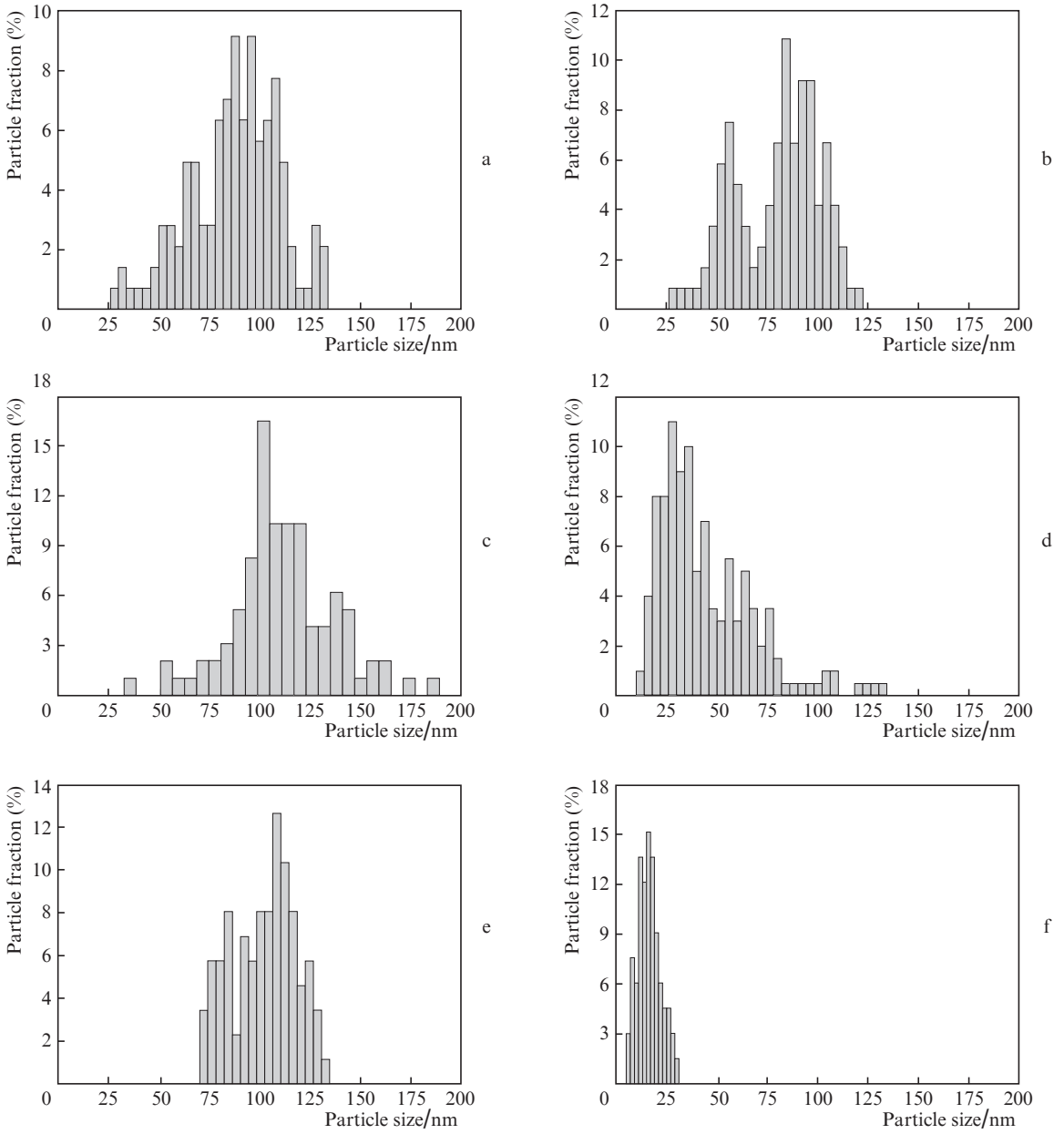

Figure 1. Histograms of the size distribution of nanoparticles formed via laser ablation of (a) PS and (b) CS in water, (c) PS and (d) CS in ethanol, and (e) PS and (f) CS in liquid nitrogen.

efficiency of agglomeration of the latter in the SNPs, which directly determines the final particle sizes, should be higher as compared with the case of using CS.

This hypothesis is also confirmed by the excess of mass concentrations of SNPs formed via ablation of porous targets, as compared to those for ablation of CS using the same buffer liquid at comparable irradiation times (Table 1). As a result of ablation in water and ethanol, the SNP mass yield after normalisation of the mass concentration for irradiation time was more than 3 times higher for PS targets as compared to the case of CS targets. During ablation in liquid nitrogen, an increase in the mass concentration of SNPs by a factor of 1.5 was observed when the CS target was replaced by a PS layer.

The presented histograms for SNPs obtained by ablation of CS (Figs 1b, 1d, and 1f) are in good agreement with the results of experiments previously conducted under similar conditions [20, 33, 34]. The bimodal size distribution of the SNPs produced by ablation of CS in water can be explained by the theory developed by Shih et al. [35]: The appearance of smaller particles is due to the fast nucleation of atoms evaporated from the target surface in the area of interaction with water molecules under continuous in time tendency towards thermodynamic equilibrium (cooling of ablation products) [21], while the larger particles originate from the presence of Richtmyer–Meshkov thermodynamic instability [36], resulting from exposure by a short laser pulse [37] and leading to a shock ejection of the melt from the overheated target in the form of nanojets, at the end of which droplets appear to agglomerate when cooled to sufficiently large nanoparticles.

The formation of SNPs with the smallest average size of 16 nm with a standard deviation of 6 nm in the case of ablation of CS in liquid nitrogen is explained by ablation at low temperature (77.4 K), which prevents the long process of interaction of ablation products with a buffer liquid and, as a result, their effective agglomeration into SNPs [19].

At the same time, a comprehensive study of the structural and optical properties of SNPs produced by femtosecond laser ablation of PS for a set of liquids considered in this work, to the best of our knowledge, is performed for the first time. The average sizes of particles formed via ablation of PS films in water, ethanol, and liquid nitrogen were 87 nm, 112 nm, and 102 nm, respectively. From the point of view of further SNP embedding into biological tissues, the obtained values are relatively high. However, it should be noted that a comparative analysis of size distributions with other works, where mechanically ground PS was studied, shows a significant gain in the case of nanostructuring by laser ablation with respect to SNP size dispersion. As a result of our experiments, SNPs produced from ablated PS have a relatively narrow size distribution: the standard deviations are 22 nm, 26 nm, and 16 for water, ethanol, and liquid nitrogen used as a buffer media for ablation, respectively (Table 1).

For further quantitative comparison with the results of studies where the SNP sizes obtained by mechanical grinding of PS were analysed based on high-resolution microscopy data, however, without numerical estimates of the standard deviation [5, 7, 10], we assessed the particle size spread relative to the average size. In other words, the size ranges were evaluated, beyond which SNPs were not detected. As a result of experiments on femtosecond laser ablation of PS in liquids, the spread value does not exceed 60 nm, 75 nm and 30 nm for water, ethanol and liquid nitrogen, respectively (Figs 1a, 1c, and 1e). The minimum spread value corresponding to a standard deviation of 16 nm (Table 1) in the latter case we, similarly to the previous discussions, associate with the formation of SNPs at the temperature of liquid nitrogen in shorter times as compared to ablation in other liquids at room temperature: The lower the temperature, the faster the cooling and the less intensive the spreading of ablation products determining, among other things, the size dispersion of the produced SNPs. It should be noted that in the case of PS mechanical grinding, even when average sizes of produced nanoparticles are about 100 nm, SNPs have noticeably wider size spread, especially towards large sizes of up to 300 nm [5, 7, 10], which can only be eliminated by additional filtration or centrifugation with separation of the fraction of large particles.

Subsequent analysis of the light absorption and scattering properties was performed on the basis of spectrophotometric measurements of the fabricated SNP suspensions without additional filtering or changes the in solution concentrations. Prior to measurements, only ultrasonic mixing of the suspensions was performed for the purpose of homogenization. The values of the absorption coefficient μ_a and reduced scattering coefficient $\mu_s' = \mu_s (1 - g)$, where μ_s is the scattering coefficient and g is the anisotropy factor, were reconstructed according to [32] from the spectra of diffuse reflectance, collimated and diffuse transmittance of the studied SNP suspensions. The results of reconstruction are presented in Figs 2 and 3.

As can be seen from Fig. 2a, the μ_a value for SNPs formed via laser ablation of PS monotonically decreases in the range 400–600 nm from values of the order of 0.1 mm^{-1} to values close to zero. This behaviour is in good agreement with the spectral dependence of silicon absorption [38, 39]. The insig-

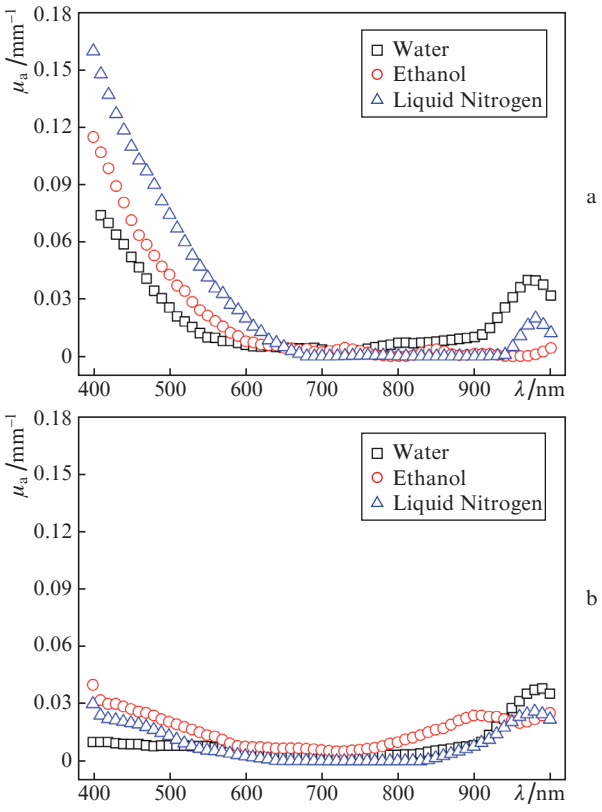

Figure 2. Spectral dependences of the absorption coefficient μ_a of SNP suspensions formed via ablation of (a) PS layers and (b) CS plates in various buffer media.

nificant absorption peak at a wavelength of 975 nm for the considered cases of ablation in water and liquid nitrogen is due to absorption in water, in which SNPs are present in the form of a suspension in both cases. At the same time, for SNPs produced and subsequently remaining in ethanol, this peak is not observed.

It should be noted that, apart from the concentration of SNPs, their size also affects the absorption of the studied suspensions. Earlier, as a result of simulation of the optical properties of the SNPs, we showed that particles with a larger size make a greater contribution to the absorption even at lower concentrations due to their high absorption cross section [7]. Therefore, for example, in the blue spectral region, the absorption coefficient of the SNP suspension formed via PS ablation in liquid nitrogen is two times higher than that for ablation in water (Fig. 2a). Although the concentration of the SNPs in the water suspension is higher for 33% than that for liquid nitrogen (Table 1), the average size of the SNPs formed in liquid nitrogen is noticeably larger than that for ablation in water: 102 nm vs. 87 nm. It is worth noting that the final product of both techniques is the water solution of SNPs, because particles ablated in liquid nitrogen are suspended in water at the final step of manufacturing. After ablation in ethanol, the SNPs remain in it, and for a comparative analysis of the contribution of particle sizes to absorption in different liquids, it is necessary to additionally take into account the difference in the contrast of the complex refractive indices at the silicon–ethanol and silicon–water interfaces.

Typical trends in the spectral dependences are repeated for nanoparticles fabricated by laser ablation of CS (Fig. 2b); however, the absolute value of the absorption coefficient in this case is less, due to the lower concentration of particles in suspension. It should be noted that the absolute value of the water absorption peak coincides for both particle samples obtained by laser ablation in water, which indicates that in the spectral range of 900–1000 nm, absorption is mainly provided by water, rather than by SNPs. It should be noted that the error of the applied optical properties reconstruction technique is at the level of 0.01 mm^{-1}.

Thus, weak absorption of the studied SNP suspensions at wavelengths above 600 nm determined by relatively high transparency of silicon in the red and near-infrared ranges [38, 39] should contribute to their effective application in light scattering based techniques for imaging of biological tissues and their phantoms in the so-called diagnostic transparency window of 700–1300 nm.

An analysis of the spectra of the reduced scattering coefficient μ'_s (Fig. 3) allows one to characterise the probability of a significant change in the direction of the photon propagating in the medium, which is important when evaluating the effectiveness of suspensions as contrasting agents for optical imaging methods, in particular, for optical coherent tomography (OCT). The spectral dependences of μ'_s for particles fabricated via ablation of PS (Fig. 3a) have a nearly monotonic decreasing trend, which is consistent with the spectral dependence of the refractive index of silicon [38]; slight deviations from monotonicity can be explained by SNP size dispersion in the studied suspensions (Fig. 1). In general, the values of the reduced scattering coefficient for PS ablation vary from 0 to 0.14 mm^{-1}. In the entire spectral range under consideration, the maximal μ'_s for ablation of PS is achieved in liquid nitrogen, and the minimal one, in water.

A similar trend persists for SNP suspensions formed via CS ablation: μ'_s values decrease depending on the used buffer liquid in the liquid nitrogen–ethanol–water order in accordance with a decrease in the size of SNPs obtained in these media (Fig. 3b). However, all the obtained values of the reduced scattering coefficient do not exceed the value of 0.025 mm^{-1}, and the dependences show a more pronounced nonmonotonic character in comparison with PS ablation. The first difference can be explained by the lower concentration and size of SNPs produced upon ablation of CS (Table 1) [7], while the second both by SNP size dispersion and measurement errors, since due to low concentrations of nanoparticles, the measurements were carried out at the technique sensitivity limit of 0.01 mm^{-1}.

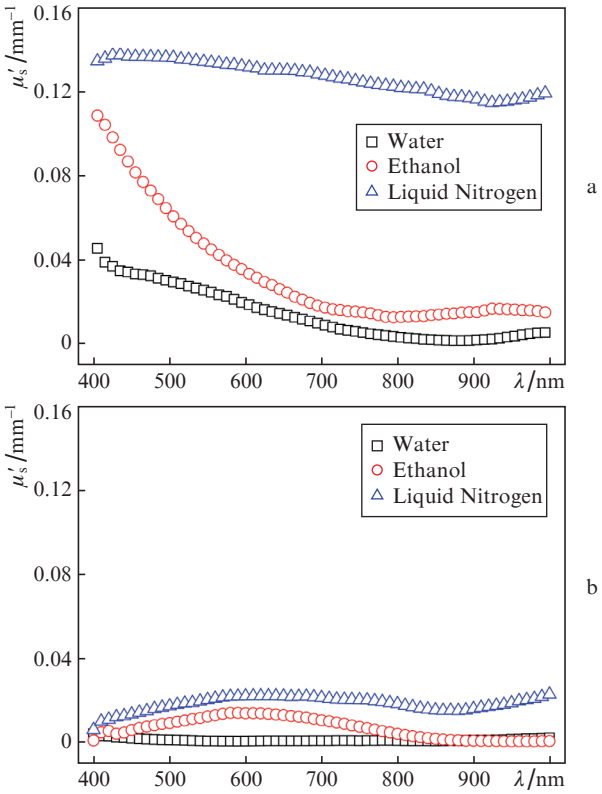

Figure 3. Spectral dependences of the reduced scattering coefficient μ'_s of SNP suspensions formed via ablation of (a) PS layers and (b) CS plates in various buffer media.

Thus, the values of the reduced scattering coefficient for SNP suspensions formed via laser ablation of PS targets exceed that for CS for several times. Therefore, the first type of particles in the framework of the study is more promising for use as contrast agents in OCT, which determined the further experiment on OCT visualisation of agar phantoms with administered suspensions of SNPs formed via laser ablation of PS layers.

The potential of using SNPs, fabricated via laser ablation, in OCT was demonstrated in our model experiments with SNPs embedded in an agar phantom. Figure 4a shows a typical image of the initial agar phantom, characterised by a small contrast value. The upper bright line corresponds to the surface of the fibre probe, while the lower line corresponds to the air–agar phantom boundary. The image below the second line corresponds to the signal from the phantom and is characterised by a low signal level, which amounted 6.3 ± 0.2 dB

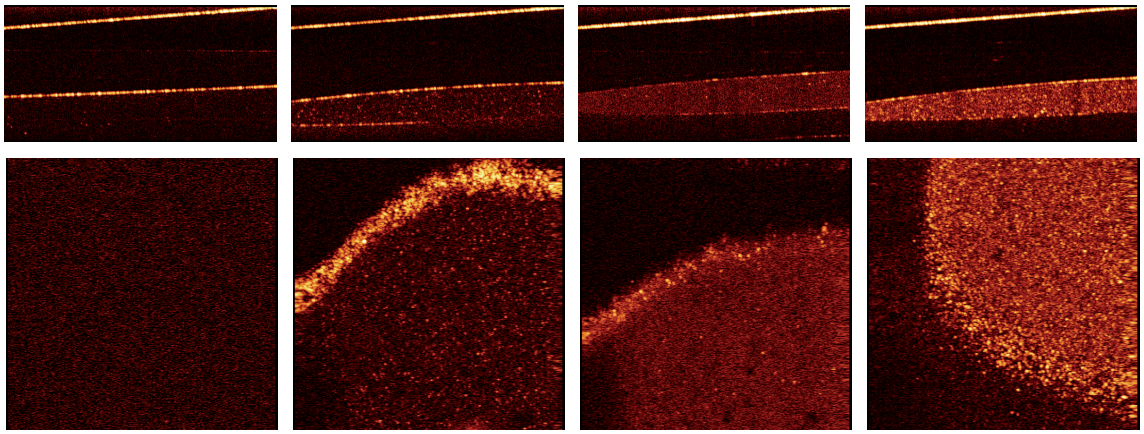

Figure 4. OCT images of a droplet of an SNP suspension (the top row shows in-depth image, and the bottom row shows enface image) on the surface of an agar phantom (a) without nanoparticles and (b–d) with administered SNPs formed by laser ablation of PS in (b) water, (c) ethanol and (d) liquid nitrogen. The size of top and bottom images are 3 × 1 mm and 3 × 3 mm, respectively.

from all used samples without SNPs. Figures 4b–4d show OCT images of the phantom after the surface administration of a droplet of a SNP suspension produced by ablation of PS in various liquids. From these images, one can see that the increase in their contrast provided by administration of SNPs is in qualitative agreement with the results of spectrophotometric measurements: The highest contrast is provided by the SNPs formed via ablation of PS in liquid nitrogen, while the lowest is for the SNPs produced in water (Table 2).

Table 2. Contrasting OCT images of an agar phantom using SNPs formed via laser ablation of PS in liquids.

Buffer medium	OCT signal from nanoparticles/dB	Contrast/dB
Water	8.6	2.2
Ethanol	11.5	5.2
Liquid hydrogen	17.1	10.9

Note: The contrast value is calculated as the difference between the signals from the phantom with and without nanoparticles.

Thus, a correlation was revealed between the reduced light scattering coefficient of administered suspension and the contrast of the OCT images of the agar gel phantom with SNPs. Despite the fact that the centre wavelength of the OCT probing wavelength (1300 nm) does not fall into the spectral range where μ_s' measurements were performed (400–1000 nm), the correlation can be considered reliable, at least for a qualitative description of the observed trends due to the monotonicity of the silicon refractive index dispersion dependences in the wavelength range of 400–1300 nm [38].

4. Conclusions

We have demonstrated the possibility of SNP formation by femtosecond laser ablation of PS. Employment of various liquids for ablation allows controlling the size distribution of fabricated SNPs: The average sizes are 87, 112 and 102 nm, and the spread does not exceed 60, 75 and 30 nm for cases of ablation in water, ethanol and liquid nitrogen, respectively. These size distributions are narrower than those obtained with the traditional method of mechanical PS grinding and, accordingly, are more preferable from the point of view of using SNPs in biomedical applications. Compared to CS, PS ablation also has an advantage in terms of a higher yield of ablation products and more efficient light scattering by SNP ensembles according to the analysis performed by gravimetric and spectrophotometric techniques, respectively.

For an agar gel-based phantom, it was shown that the SNPs formed via laser ablation of PS can be effectively employed for contrasting OCT images. A correlation was found between the values of the reduced light scattering coefficient, which depend on the buffer liquid, and the contrast value of the OCT images: the higher the μ_s' value, the better the achieved contrast.

Acknowledgements. The authors thank O.O. Chura for his help with gravimetric measurements.

This work was supported by the Russian Science Foundation (Grant No. 19-12-00192).

References

1. Park J.-H., Gu L., von Maltzahn G., Ruoslahti E., Bhatia S.N., Sailor M.J. *Nature Mater.*, **8** (4), 331 (2009).
2. Ksenofontova O.I., Vasin A.V., Egorov V.V., Bobyl A.V., Soldatenkov F.Yu., Terukov E.I., Ulin V.P., Ulin N.V., Kiselev O.I. *Tech. Phys.*, **59** (1), 66 (2014) [*Zh. Tekh. Fiz.*, **84** (1), 67 (2014)].
3. Stojanovic V., Cunin F., Durand J.O., Garcia M., Gary-Bobo M. *J. Mater. Chem. B*, **4**, 7050 (2016).
4. Baati T., Al-Kattan A., Esteve M.-A., Njim L., Ryabchikov Yu., Chaspoul F., Hammami M., Sentis M., Kabashin A.V., Braguer D. *Sci. Rep.*, **6**, 25400 (2016).
5. Tolstik E., Osminkina L.A., Matthäus C., Burkhardt M., Tsurikov K.E., Natashina U.A., Timoshenko V.Yu., Heintzmann R., Popp J., Sivakov V. *Nanomedicine: NBM*, **12**, 1931 (2016).
6. Kirillin M.Yu., Sergeeva E.A., Agrba P.D., Krainov A.D., Ezhov A.A., Shuleiko D.V., Kashkarov P.K., Zabotnov S.V. *Laser Phys.*, **25** (7), 075604 (2015).
7. Zabotnov S.V., Kashaev F.V., Shuleiko D.V., Gongalsky M.B., Golovan L.A., Kashkarov P.K., Loginova D.A., Agrba P.D., Sergeeva E.A., Kirillin M.Yu. *Quantum Electron.*, **47** (7), 638 (2017) [*Kvantovaya Elektron.*, **47** (7), 638 (2017)].
8. Krainov A.D., Agrba P.D., Sergeeva E.A., Zabotnov S.V., Kirillin M.Yu. *Quantum Electronics*, **44** (8), 757 (2014) [*Kvantovaya Elektron.*, **44** (8), 757 (2014)].

9. Lee C., Kim H., Hong C., Kim M., Hong S.S., Lee D.H., Lee W.I. *J. Mater. Chem.*, **18**, 4790 (2008).
10. Hong C., Lee J., Zheng H., Hong S.-S., Lee C. *Nanoscale Res. Lett.*, **6**, 321 (2011).
11. Tamarov K.P., Osminkina L.A., Zinovyev S.V., Maximova K.A., Kargina Ju.V., Gongalsky M.B., Ryabchikov Yu., Al-Kattan A., Sviridov A.P., Sentis M., Ivanov A.V., Nikiforov V.N., Kabashin A.V., Timoshenko V.Yu. *Sci. Rep.*, **4**, 7034 (2014).
12. Secret E., Maynadier M., Gallud A., Chaix A., Bouffard E., Gary-Bobo M., Marcotte N., Mongin O., Cheikh K.E., Hugues V., Auffan M., Frochot C., Morère A., Maillard P., Blanchard-Desce M., Sailor M.J., Garcia M., Durand J.-O., Cunin F. *Adv. Mater.*, **26**, 7643 (2014).
13. Xiao L., Gu L., Howell S.B., Sailor M.J. *ACS Nano*, **5** (5), 3651 (2011).
14. Chaix A., Cheikh K.E., Bouffard E., Maynadier M., Aggad D., Stojanovic V., Knezevic N., Garcia M., Maillard P., Morère A., Gary-Bobo M., Raehm L., Richeter S., Durand J.-O., Cunin F. *J. Mater. Chem. B*, **4**, 3639 (2016).
15. Sviridov A.P., Osminkina L.A., Kharin A.Yu., Gongalsky M.B., Kargina J.V., Kudryavtsev A.A., Bezsudnova Yu.I., Perova T.S., Geloen A., Lysenko V., Timoshenko V.Yu. *Nanotechnology*, **28**, 105102 (2017).
16. Loni A., in *Handbook of Porous Silicon* (Basel: Springer, 2018) pp 13–24.
17. Al-Kattan A., Ryabchikov Yu.V., Baati T., Chirvony V., Sánchez-Royo J.F., Sentis M., Braguer D., Timoshenko V.Yu., Estève M.-A., Kabashin A.V. *J. Mater. Chem. B*, **4**, 7852 (2016).
18. Ryabchikov Yu.V. *Phys. Status Solidi A*, **216** (2), 1800685 (2019).
19. Perminov P.A., Dzhun I.O., Ezhov A.A., Zabotnov S.V., Golovan L.A., Ivlev G.D., Gatskevich E.I., Malevich V.L., Kashkarov P.K. *Laser Phys.*, **21** (4), 801 (2011).
20. Eroshova O.I., Perminov P.A., Zabotnov S.V., Gongalsky M.B., Ezhov A.A., Golovan L.A., Kashkarov P.K. *Crystallogr. Rep.*, **57**, 831 (2012) [*Kristallogr.*, **57** (6), 942 (2012)].
21. Petrov Yu.I. *Klastery i malye chastitsy* (Clusters and Small Particles) (Moscow: Nauka, 1986).
22. Blandin P., Maximova K.A., Gongalsky M.B., Sanchez-Royo J.F., Chirvony V.S., Sentis M., Timoshenko V.Yu., Kabashin A.V. *J. Mater. Chem. B*, **1** (19), 2489 (2013).
23. Gongalsky M.B., Osminkina L.A., Pereira A., Manankov A.A., Fedorenko A.A., Vasiliev A.N., Solovyev V.V., Kudryavtsev A.A., Sentis M., Kabashin A.V., Timoshenko V.Yu. *Sci. Rep.*, **6**, 24732 (2016).
24. Rioux D., Laferriere M., Douplik A., Shah D., Lilge L., Kabashin A.V., Meunier M.M. *J. Biomed. Opt.*, **142**, 021010 (2009).
25. Ryabchikov Yu.V., Belogorokhov I.A., Vorontsov A.S., Osminkina L.A., Timoshenko V.Yu., Kashkarov P.K. *Phys. Status Solidi A*, **204** (5), 1271 (2007).
26. Konstantinova E.A., Demin V.A., Vorontzov A.S., Ryabchikov Yu.V., Belogorokhov I.A., Osminkina L.A., Forsh P.A., Kashkarov P.K., Timoshenko V.Yu. *J. Non-Cryst. Solids*, **352**, 1156 (2006).
27. Golovan L.A., Djun I.O., Dokukina A.E., Zabotnov S.V., Ezhov A.A., Kashkarov P.K., Maslova N.E., Ostapenko I.O., Panov V.I., Timoshenko V.Yu. *Bull. Russ. Acad. Sci.: Phys.*, **73**, 39 (2009) [*Izv. Ross. Akad. Nauk, Ser. Fiz.*, **73** (1), 43 (2009)].
28. Rouquerol J., Avnir D., Fairbridge C.W., Everett D.H., Haynes J.H., Pernicone N., Ramsay J.D.F., Sing K.S.W., Unger K.K. *Pure Appl. Chem.*, **66**, 1739 (1994).
29. Agranat M.B., Ashitkov S.I., Ivanov A.A., Konyashchenko A.V., Ovchinnikov A.V., Podshivalov A.A. *Quantum Electron.*, **34** (11), 1018 (2004) [*Kvantovaya Elektron.*, **34** (11), 1018 (2004)].
30. Gordienko V.M., Ivanov A.A., Podshivalov A.A., Savel'ev A.B., Rakov E.V. *Laser Phys.*, **16** (3), 427 (2006).
31. Akhmanov S.A., Nikitin S.Yu. *Physical Optics* (New York: Clarendon Press, 1997; Moscow: Nauka, 2004).
32. Skobelkina A.V., Kashaev F.V., Kolchin A.V., Kaminskaya T.P., Zabotnov S.V., Golovan L.A., Loginova D.A., Khilov A.V., Agrba P.D., Kirillin M.Yu. *Memoirs of the Faculty of Physics*, **4**, 1841302 (2018).
33. Intartaglia R., Bagga K., Brandi F., Das G., Genovese A., Di Fabrizio E., Diaspro A. *J. Phys. Chem. C*, **115**, 5102 (2011).
34. Kuzmin P.G., Shafeev G.A., Bukin V.V., Garnov S.V., Farcau C., Carles R., Warot-Fontrose B., Guieu V., Viau G. *J. Phys. Chem. C*, **114**, 15266 (2010).
35. Shih C.-Yu., Streubel R., Heberle J., Letzel A., Shugaev M.V., Wu C., Schmidt M., Gökce B., Barcikowski S., Zhigilei L.V. *Nanoscale*, **10**, 6900 (2018).
36. Brouillette M. *Ann. Rev. Fluid Mech.*, **34**, 445 (2002).
37. Dyachkov S.A., Zhakhovsky V.V., Parshikov A.N., Inogamov N.A. *J. Phys. Conf. Ser.*, **1147**, 012064 (2019).
38. Philipp H.R., Taft E.A. *Phys. Rev.*, **120** (1), 37 (1960).
39. Schinke C., Peest P.C., Schmidt J., Brendel R., Bothe K., Vogt M.R., Kröger I., Winter S., Schirmacher A., Lim S., Nguyen H.T., MacDonald D. *AIP Advances*, **5**, 67168 (2015).